Numerical modeling of solidification process during continuous casting including the effects of interface heat flux

by Nikhil Lingaji Gawas

A thesis submitted in partial fulfillment of the requirements for the degree of Master of Science in Mechanical Engineering
Montana State University

Abstract:
Multiphase fluid flow involving solidification is common in many industrial processes like extrusion, continuous casting, drawing, etc. Thus, thermal transport is significant in these cases. The present study concentrates on the study of air gap formation on the metal-mold interfacial heat transfer of a continuous casting mold. The numerical modeling of continuous casting has attained a sophisticated level by including other phenonmenon which take place during the process. Solidification models include metal-mold interfacial heat transfer, mold distortion, macrosegregation, turbulence and argon gas injection to name a few.

The present method takes into account the shrinkage of the metal when it undergoes cooling in the metal mold by losing latent heat as well as sensible heat. The formulation for the air gap formation was assumed one-dimensional with conduction as the only mode of transfer in the air gap. The metal-mold interfacial air gap was converted into an effective heat resistance which is incorporated on the outer surface of the mold by changing the convective heat transfer coefficient.

Initially, an algorithm was developed and validated to simulate the basic process. This algorithm was modified to include the effect of air gap based on the shrinkage formulation. The parameters were studied to comprehend the effect of air gap heat resistance on different aspects of the process. Basic process variables were the superheat temperature or the inlet temperature, withdrawal velocity and the mold/post mold cooling rates. The results were non-dimensionalized to generalize them for comparison. Results were plotted in terms of solidification front, average and local heat flux, mold wall temperature, centerline temperature, velocity vector and fractional heat extracted in the mold.

A few cases were also run with and without air gap modeling and their results compared. It was noted that a small value of air gap width significantly affected the heat transfer. The air gap width was critical, as in some cases the gap was too small to affect the total heat flux. The current study shows that there exists a limiting value of withdrawal speed (Pe) and superheat (θ0) above which the effect of air gap formation on the overall heat transfer is negligible. A critical value of mold cooling rate (Bi2) also exists for a given set of parameters, which gives the maximum heat extraction rate. The effect of post mold cooling rate (Bi3) on the overall heat transfer was negligible.

NUMERICAL MODELING OF SOLIDIFICATION PROCESS DURING CONTINUOUS CASTING INCLUDING THE EFFECTS OF INTERFACE HEAT FLUX

by

Nikhil Lingaji Gawas

A thesis submitted in partial fulfillment
of the requirements for the degree

of

Master of Science

in

Mechanical Engineering

MONTANA STATE UNIVERSITY
Bozeman, Montana

March 2001

APPROVAL

of a thesis submitted by

Nikhil Gawas

This thesis has been read by each member of the thesis committee and has been found to be satisfactory regarding content, English usage, format, citations, bibliographic style, and consistency, and is ready for submission to the College of Graduate Studies.

Dr. Ruhul Amin _____ (Signature) 8 March 2001 Date

Approved for the Department of Mechanical and Industrial Engineering

Dr. Vic Cundy _____ (Signature) 3/9/01 Date

Approved for the College of Graduate Studies

Dr. Bruce R. McLeod _____ (Signature) 3-9-01 Date

STATEMENT OF PERMISSION TO USE

In presenting this thesis in partial fulfillment of the requirements for a master's degree at Montana State University, I agree that the Library shall make it available to borrowers under rules of the Library.

If I have indicated my intention to copyright this thesis by including a copyright notice page, copying is allowable only for scholarly purposes, consistent with "fair use" as prescribed in the U.S. Copyright Law. Requests for permission for extended quotation from or reproduction of this thesis in whole or in parts may be granted only by the copyright holder.

Signature M Ganvas

Date March 09, 2001

ACKNOWLEDGMENTS

I would like to thank Dr. Ruhul Amin for his guidance in my research and thesis work. I would also like to thank Dr. Alan George and Dr. Thomas Reihman for their work as committee members.

Dr. Ladean McKittrick deserves a special mention for helping me out with the computing resources. I also appreciate the Department of Mechanical and Industrial Engineering and my parents for providing me with financial assistance.

Finally, my appreciation goes out to all the staff of the Department of Mechanical and Industrial Engineering and my fellow graduate students for their continued support.

TABLE OF CONTENTS

TABLE OF CONTENTS - Continued

LIST OF TABLES

LIST OF FIGURES

LIST OF FIGURES – continued

LIST OF FIGURES – continued

LIST OF FIGURES – continued

LIST OF FIGURES – continued

NOMENCLATURE

Symbol	Description
Ar	Aspect ratio of cast material, L / W
Bi	Biot number
Bi_1	Pre-mold region Biot number
Bi_2	Mold Biot number $= h_2 W / k_{Cu}$
Bi_3	Post-mold Biot number $= h_3 W / k_{Cu}$
C	Specific heat
C_ϕ	Diffusion coefficient
g	constant of gravity.
h	Heat transfer coefficient
h_2	Dimensional mold convective heat transfer coefficient
h_3	Dimensional post-mold convective heat transfer coefficient
H^*	Non-dimensional effective heat transfer coefficient
H_{eff}	Effective heat transfer coefficient
k	Thermal conductivity
L	Length of the cast material
L_h	Latent heat of fusion
L_1	Length of pre-mold region
L_2	Length of mold region
L_3	Length of post-mold region
P	Pressure

NOMENCLATURE – continued

Pe	Peclet number = U_0W / α_s
q	Local heat flux
q^*	Non-dimensional local heat flux
Q^*	Average dimensionless heat flux
R	Resistance
r^2	Variance of data
Ste	Stefan number = $C_s (T-T_\infty) / L_h$
t	time
t_m	thickness of the copper mold
T	Temperature
T_0	Temperature at the inlet
T_s	Solidification temperature of Aluminum
T_∞	Ambient temperature
U_0	Withdrawal speed.
V_x	X component of velocity
V_y	Y component of velocity
W	Half thickness of the cast material
W^e	Weighting function
X_{gap}	Air gap width

Greek Symbols

α	Thermal diffusivity (also coefficient of linear expansion where stated)

NOMENCLATURE – continued

β	Coefficient of volumetric expansion
δ	Dirac-delta-function (also temperature difference wherever mentioned)
μ	Dynamic viscosity
ρ	Density
θ	Non-dimensional temperature = $(T-T_\infty)/(T_s - T_\infty)$
ϕ	Degree of freedom variable (DOF)
Γ	Diffussion Coefficient
τ	Stress tensor
λ	Second coefficient of viscosity
Δ	Mathematical operator for difference

Subscripts and Superscripts

avg	Average value
Al	Aluminum
Cu	Copper
d	downwind nodes
e	element property
eff	effective value
gap	air gap property
l	liquid phase
m	mold property
s	solid property

NOMENCLATURE – continued

u	upwind nodes
0	condition at the inlet

Ansys commands nomenclature

FLDATA	Specifies various fluid properties
MAT	Specifies material properties
MP	Specifies material properties table
MPDATA	Specifies data for material properties table
KEYOPT(1)	Activates multiple species transport
KEYOPT(3)	Specifies the coordinate system

ABSTRACT

Multiphase fluid flow involving solidification is common in many industrial processes like extrusion, continuous casting, drawing, etc. Thus, thermal transport is significant in these cases. The present study concentrates on the study of air gap formation on the metal-mold interfacial heat transfer of a continuous casting mold. The numerical modeling of continuous casting has attained a sophisticated level by including other phenonmenon which take place during the process. Solidification models include metal-mold interfacial heat transfer, mold distortion, macrosegregation, turbulence and argon gas injection to name a few.

The present method takes into account the shrinkage of the metal when it undergoes cooling in the metal mold by losing latent heat as well as sensible heat. The formulation for the air gap formation was assumed one-dimensional with conduction as the only mode of transfer in the air gap. The metal-mold interfacial air gap was converted into an effective heat resistance which is incorporated on the outer surface of the mold by changing the convective heat transfer coefficient.

Initially, an algorithm was developed and validated to simulate the basic process. This algorithm was modified to include the effect of air gap based on the shrinkage formulation. The parameters were studied to comprehend the effect of air gap heat resistance on different aspects of the process. Basic process variables were the superheat temperature or the inlet temperature, withdrawal velocity and the mold/post mold cooling rates. The results were non-dimensionalized to generalize them for comparison. Results were plotted in terms of solidification front, average and local heat flux, mold wall temperature, centerline temperature, velocity vector and fractional heat extracted in the mold.

A few cases were also run with and without air gap modeling and their results compared. It was noted that a small value of air gap width significantly affected the heat transfer. The air gap width was critical, as in some cases the gap was too small to affect the total heat flux. The current study shows that there exists a limiting value of withdrawal speed (Pe) and superheat (θ_0) above which the effect of air gap formation on the overall heat transfer is negligible. A critical value of mold cooling rate (Bi_2) also exists for a given set of parameters, which gives the maximum heat extraction rate. The effect of post mold cooling rate (Bi_3) on the overall heat transfer was negligible.

CHAPTER 1

INTRODUCTION

Thermal transport phenomenon plays an important role in engineering applications especially in manufacturing processes such as continuous casting, optical fiber drawing, hot rolling and metal wire drawing.

Continuous casting is a rapidly developing field and has gained prime importance in the manufacturing of ferrous and non-ferrous slabs. A substantial amount of steel produced every year is by way of continuous casting. Figure 1 shows a typical setup of a continuous casting mill.

Superheated metal enters a metal mold, which is open ended, via a tundish and a nozzle. The metal is cooled due to heat exchange with the mold, which is water-cooled. As the metal shell forms, it is continuously withdrawn from the exit of the mold with the help of pinch rollers. Lubrication is provided with the help of mold flux, which prevents the liquid metal from sticking to the mold wall. On exit, the metal shell is subjected to spray cooling before finally being cut off by a gas torch.

Serious problems are encountered during continuous casting if the process parameters are not carefully monitored and controlled. The heat extraction rate and the withdrawal speed are particularly critical, for if they are not controlled, it can lead to breakout. Breakout is a serious condition where the metal shell formed cannot withstand the ferrostatic pressure of the liquid core, and due to insufficient shell thickness, the solid metal breaks spilling out hot liquid metal. This leads to formidable damages and repairs. Other defects include air-gap formation at the metal-mold interface due to thermal

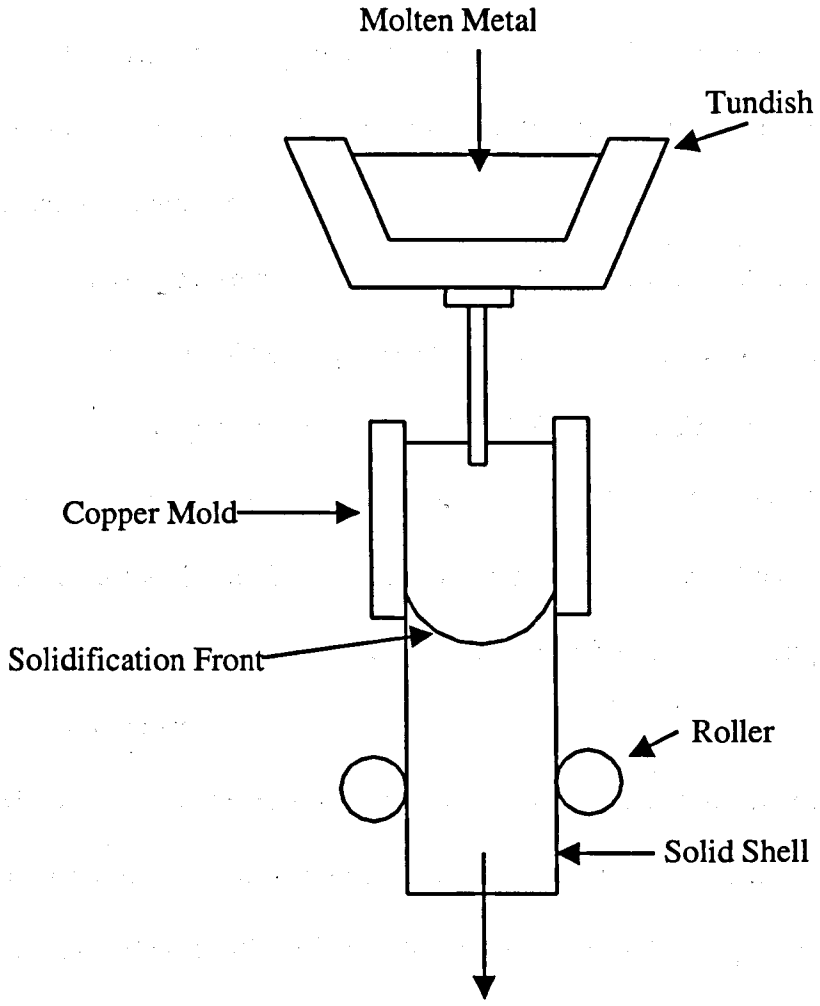

Figure 1. Continuous Casting Setup.

shrinkage, rhombodity and corner cracks due to mold distortion as reported by Samarasekara and Brimacombe (1979,1984), residual stresses due to uneven cooling and surface depressions.

Motivation

Optimization and process control are of prime importance to reduce defects and increase productivity. Correspondingly, numerical modeling of continuous casting has received more attention, complemented by the fact that it is less expensive compared to experimental investigation.

Parameters governing the process need to be studied carefully in order to streamline the process. Typical parameters include superheat temperature, withdrawal velocity, mold cooling rate and post-mold cooling rate. Present research is primarily focused on the effects of air gap formation on the mold-metal interfacial heat transfer. Air gap at the metal-mold interface leads to decreased contact conductance, thus decreasing the overall effective heat transfer thereby leading to higher mold temperatures and lower heat transfer efficiency.

Mold heat transfer is governed by the size of the gap separating the solidifying shell from the wall of the cooling mold and the properties of the flux which infiltrates the gap. Biloni and Prates (1977) have shown that even when liquid metal makes contact with the mold wall, there is some contact resistance. Irwing (1967) has studied interfacial heat transfer in the case of ingot molds. He has seen that for air gap values up to 100μm, heat transfer takes place mainly due to conduction through air and radiation was negligible. For air gaps above 100μm, radiation becomes appreciable only when casting surface temperatures are above 800°C. The gap width and mold heat extraction are also dependent on the characteristics of the oscillation marks present on the slab surface. An

oscillation mark locally increases the gap, reduces heat transfer to the mold, and retards shell growth. Deep oscillation marks can be deleterious for surface quality because they are frequently the site of transverse cracks. Thus, understanding interfacial heat transfer is highly desirable in the event of air-gap formation.

It is important to predict quantitatively and understand qualitatively various phenomena involved in continuous casting process. Air gap formation is a hindrance to the process and understanding how and where it forms is an important step towards its prevention. Although information is available on the metal-mold interface heat transfer for metal ingot castings, hardly any data could be found regarding the same in continuous castings for pure metals. Hence, aluminum was chosen for modeling, although steel remains the major material manufactured by continuous casting process.

Background

Numerical modeling of thermo-fluid applications has been in the cynosure due to rapid development in computing. Faster computing and large memory space gives an opportunity to do analyses previously thought to be time consuming and practically impossible. Finite difference methods, finite volume methods and finite element methods are commonly used to tackle any computational fluid dynamics (CFD) problem.

Phase change problems are highly non-linear due to the presence of a boundary (solidification front) across which the properties vary like Dirac-δ-type behavior (especially for pure substances). The class of problems usually referred to as 'isothermal phase change' problems pose greater computational difficulties. In such problems, the numerical simulations for the temperature history and/or the location of the solidification front result in some sort of overprediction / underprediction as well as numerical oscillations about the true response as pointed out by Namburu and Tamma (1990). Finite difference methods were traditionally employed for analyzing the phase change problems. Currently, numerical analysts are focusing more on finite element analysis (FEA) due to their inherent advantages in handling the evolution of latent heat. By employing finite elements in conjunction with numerical integration, a reasonable accuracy can be obtained for sufficiently smooth variations of the effective heat transfer capacity as reported by Namburu and Tamma (1990). In this research the enthalpy method has been employed and will be discussed in the following chapters.

Numerical modeling of continuous casting dates back almost five decades. Many researchers have contributed to the mathematical modeling of continuous casting process. Primarily two approaches have been adopted to solve this problem numerically; one is the moving grid technique and the second is the fixed grid technique. The fixed grid technique handles the latent heat evolution by introducing non-linearities in the specific heat or enthalpy of the material, whereas, the moving grid technique involves the change of grid points with time.

Jaluria (1992) has presented detailed work on the thermal transport of continuously moving material. The work was focused on the conjugate problem of heat transfer and fluid flow in moving material. Boundary layer formulation and the solution to the full governing equations were devised. Several other phenomena like thermal buoyancy, transient effects and forced flow were also considered. The results were generalized and interpreted for various thermal transport processes like extrusion, fiber drawing, electric furnace heating, thermal processing of glass and continuous casting.

Kang and Jaluria (1993) have developed a thermal model of the continuous casting process. One-dimensional three-zone model and two-dimensional enthalpy model were presented. The one-dimensional model was fairly idealized and can be used for the validation of multi-dimensional models that may be employed for more complicated situations. The enthalpy model solved the equations by finite difference methods using the alternating direction implicit (ADI) scheme. It was shown that varying the governing parameters could control the shape of the solidification front. Results followed the

expected trend of the process. (i.e. the solidification front moved downstream as superheat / withdrawal speed was increased or as the cooling rates were decreased.)

Choudary and Mazumdar (1994) proposed a steady state, two-dimensional model for continuous casting. The model also included turbulence, fluid flow and thermal transport within the mushy zone and the bulk motion of the descending strand on liquid steel. The mushy zone was modeled considering the enhanced resistance offered by the dendrites by increasing the viscosity of the liquid steel. A constant apparent viscosity equal to twenty times the molecular viscosity of steel was taken. The numerical scheme employed a control volume based finite difference procedure and incorporated the SIMPLE algorithm of Patankar and Spalding (1972). The numerical results were compared with three different billet-casting operations. Shell thickness values were in good agreement with the experimental data. The comparison of results also displayed the inadequacy of the effective thermal conductivity model presented by Choudary et al. (1993).

Simulation of solidification in continuous casting of steel billets using the non-linear heat conduction equation was presented by Vanaparthy and Srinivasan (1994). A numerical method was used which employed the two-time level Crank Nicholson scheme to start the simulation, whereas Gauss-integration was used to compute the element matrices numerically. The initial conditions provided the values for generating temperatures for the first time step. The model calculated the solid shell temperatures in a transverse cross section of the billet at discrete time intervals. The influence of spray

water flux (post-mold cooling) on the amount of reheat at the corner of the billet was particularly interesting. It was shown that reheating could be minimized by decreasing the amount of water gradually from 170 GPM to 50 GPM for the given set of process parameters.

Thomas et al. (1990, 1996) investigated the effect of superheat on the fluid flow and temperature distribution in a continuous slab-casting process. The models developed included two-dimensional as well as three-dimensional domains. The solidification model was not coupled with the fluid flow and heat transfer within the caster. Instead, the velocity vector field and the temperature distribution was first obtained and then the heat flux at the wall was used in the one-dimensional solidification model to give the growth rate of the solidifying shell.

Seyedein and Hasan (1997) have presented a comprehensive three-dimensional model which couples turbulent flow and macroscopic solidification heat transfer for a continuous slab caster. The turbulence modeling involved the implementation of the standard two-equation k-ε model whereas solidification was formulated using the enthalpy method. The mushy zone was accounted for by applying the D'arcy laws for a porous media. An important conclusion drawn was that, due to wide variations of turbulent viscosity within the caster, the approach of applying an artificially enhanced melt viscosity was not acceptable. It was also found that the inlet superheat has minimal effect on the growth rate of the solid shell and the mushy zone except for the vicinity of the jet impingement region.

As our understanding of the continuous casting process increases, mathematical models are becoming more sophisticated so more of the known phenomenon can be included in the models. Various process defects have been implemented in conjunction with the basic models as well as other complex models to simulate the process aptly.

Royzman (1997) has studied the friction between strand and mold during continuous casting. He developed a mathematical model to compute the friction coefficient between the slab and the mold based on the process parameters and the properties of the mold lubricating powder in liquid and solid states. It was found that the coefficient of friction increases with an increase in casting speed whereas it decreases with increase in the mold oscillation frequency and the depth of the liquid slag layer. The atomic mass of the lubricating powder was found to have profound effect on the mold friction. Smaller atomic mass of the powder lead to lower frictional resistance.

Nakato et al. (1984) investigated the formation of shell and longitudinal cracks in mold during high speed continuous casting of slabs. The probability of occurrence of breakout as well as surface defects is high in the case of high speed casting as more liquid is flowing through the core of the solid shell. Extensive experimentation was carried out and the results were interpreted to countermeasure the formation of cracks. The measured shell profiles and those calculated mathematically were found to be in good agreement. Casting speed and powder properties had the greatest influence on the mean heat flux in the mold.

One of the significant defects that have been addressed is the air gap formation at the metal mold interface. Metal shrinkage leads to the development of an air gap at the metal mold interface leading to a considerable decrease in the heat transfer. Many researchers have attempted to characterize this phenomenon. Application of inverse techniques was one of the common methods used to quantify the contact conductance. Inverse techniques are usually used where the temperature profile is known and it is used to back calculate the heat transfer coefficient. Brimacombe et al. (1992) have used a sequential algorithm for the solution of inverse heat conduction problem (IHCP) to determine the response of both the surface heat flux and the surface temperature of flat stainless steel samples subjected to water quenching under controlled laboratory conditions that ensured one-dimensional flow.

Mechanism of heat transfer at a metal mold interface was studied by Ho and Pehlke (1984) for ingot casting. They reported that as solidification progressed the metal and mold may stay in contact along isolated asperities on the microscopically rough surfaces or an interfacial gap may gradually develop. Three different mechanisms were expected to affect the transition of a metal-mold solid contact to an interfacial gap, namely, surface interaction of the metal and the mold, transformation of metal and mold materials and effects of the geometry. A numerical procedure was also presented which was based on the non-linear technique of Beck (1970) and an implicit formulation of the enthalpy method. An implicit finite difference scheme was selected because of the absence of a stability limit in the choice of time steps. Ho and Pehlke (1985) have also

conducted experimental study of aluminum castings in metallic molds. It was demonstrated that the solidification time was highly sensitive to a change in interfacial thermal conductance in the case of metallic molds. In the case of sand castings, it was noted that the use of Chvorinov's rule [Ho and Pehlke (1985)] was an effective alternative to numerical simulation provided that the interfacial thermal conductance was sufficiently high.

Huang et al. (1992 a) presented the conjugate gradient method for the inverse solution to determine unknown contact conductance during metal casting. The advantage of the conjugate gradient method was that there was no need to assume a specific functional form over the specific domain. The method was found to be stable and converged over an order of magnitude faster than the least squares methods. An inverse analysis of heat conduction involving phase change was employed for accurate determination of air gap resistance from the transient temperature measurements taken inside the casting region and at the outer mold surface. The results showed that the method requires much less computer time than the least squares methods and was less sensitive to the measurement errors. In the function estimation approach considered, a total of 80 unknowns were estimated to establish the unknown functional form of contact conductance; whereas in the least squares method four parameters were used to represent the function.

Isaac et al. (1985) simulated the solidification of aluminum in cast iron mold using experimental values of air gap. The values of heat transfer coefficient at the casting

mold interface and at the outside mold surface were obtained from the simulation. Contact resistance, mold coating thickness and the actual air gap were the three factors considered in the calculation of heat transfer coefficient at the mold-casting interface. It was found that the value of heat transfer coefficient at the interface was not constant, but varies with time. It decreases as solidification proceeds. Also, the heat transfer due to radation contributed to about 5 percent while the rest was mainly by conduction.

Various types of one-dimensional techniques exist for estimating the size gap that forms at the interface. Droste et al. (1986) formulated a method based on the thermoelasticity equations. The temperature field and thermal expansion characteristics of the metal and mold surfaces in contact were used to calculate the displacements of both surfaces.

Commonly used expressions for evaluating the metal-mold heat transfer coefficient or the heat flux were compiled by Brimacombe et al. (1995), which are listed in Table 1. These expressions have been developed by various researchers listed in the aforementioned publication. Various factors involved in metal-mold interfacial heat transfer in a solidification problem have been considered in these expressions. Some of the common phenomena incorporated are conduction and / or radiation, transient effects and chill properties to name a few. Extensive information regarding the formulations could be found in the references listed by Brimacombe et al. (1995).

Most of the work done on interfacial heat transfer was found on ingot mold casting where the inverse problem solution was attempted. However, it provided the

necessary insight in model formulation in the present research. As pointed out by Thomas (1991), continuous casting poses a significant challenge in implementing inverse techniques as it is difficult to obtain the temperature distribution by experimentation due to shortcomings in controlling the operating variables independently.

Table 1. Expressions for evaluation of heat transfer coefficient and heat flux.

Expression for h	Remarks
$h = h_s + h_g + h_r$	Conduction and radiation considered
$h = \frac{k_g}{(x_g + s_1 + s_2)}$	Only conduction is considered
$h = \frac{\sigma(T_c + T_m)(T_c^2 + T_m^2)}{\left(\frac{1}{\varepsilon_c} + \frac{1}{\varepsilon_m} - 1\right)}$	Only radiation is considered
$h = \frac{h'}{2\sqrt{t}}$	Transient case where interfacial gap forms
$h = a + bt$	Transient h where intimate contact at interface is enhanced
$h = \frac{k}{a}\left(\frac{r\sin\theta}{y} + \frac{a - \sin\theta}{y_f}\right) = \frac{k}{y_{eq}}$	Radiation is neglected
$q_{\max} = C_1 (X_m / \alpha_m)^{n1}$	q_{max} depends on chill properties
$(q / q_{\max}) \alpha_m^{0.05} = C_2 t^{n_2}$	q declines parabolically with time

Ho (1992) has characterized the metal mold interfacial heat transfer in continuous casting of slabs. A continuous casting model was formulated based on a spreadsheet program. This model was coupled with the interface model to integrate the phenomenon. A relationship characterizing the temperature dependency of mold flux viscosity was introduced and incorporated in the fluid flow equations for liquid mold flux. Also, the fluid flow equations coupled with heat transfer equations and a mass balance on the entire flux layer was solved to obtain the flux film thickness. The heat flux across the gap was then obtained from the flux film thickness.

Pioneering work in the field of continuous casting has been carried out by Samarasekara, Brimacombe (1991, 1992, 1995, 1996) and Thomas (1990, 1991, 1996) along with other researchers. Briamcombe et al. (1991) have determined axial heat flux profiles quantitatively from temperature measurements conducted on a slab mold under routine operating conditions. They have reported that the decline of heat flux below the meniscus was due to increase in resistance to heat flow across the gap and through the solidifying shell. The shell resistance was determined from the pool profile predicted with a one-dimensional solidification model using the heat flux values to characterize the surface boundary condition. The resistance of the gap was computed by considering the combined resistances of the shell, mold wall, and cooling water/mold wall interface.

Brimacombe et al. (1996) has proposed that the process of continuous casting should be explored through the development of advanced systems such as an 'intelligent

mold'. Brimacombe and coworkers conducted industrial trials by instrumenting the mold with thermocouples, load cells and differential transducers to investigate various aspects of the steel billet casting. The mold taper was found to have a significant effect on the heat transfer. Smaller tapers resulted in higher heat flux which was attributed to the fact that there was greater mechanical interaction between the mold and shell during the negative strip in the mold oscillating cycle.

Extensive research is being conducted at the Continuous Casting Consortium at the University of Illinois, Urbana-Champagne, lead by B. G. Thomas, in formulating sophisticated continuous casting models, which include mold distortion, interfacial heat transfer, macrosegregation, taper design, stress prediction, turbulence, etc.

Coupling sophisticated models to include various aspects of the process like turbulence, etc. in the basic formulation of continuous casting compromises the efficiency of the numerical study. Extensive studies have been conducted to include all kinds of process parameters but at the expense of computational time and space. Thus, the process of continuous casting entails efficient and simple models to simulate the phenomena realistically. Simplified formulations have to be explored and their results compared, to benchmark the adequacy of the models. Therefore, a simple one-dimensional conduction model was formulated in the present research for investigating the interfacial heat flux, which will be discussed in the following chapters. The two dimensional governing equations were solved using a finite element method.

CHAPTER 2

PROBLEM FORMULATION

Concept

In continuous casting process, molten metal enters a mold which is open ended and flows down the mold. The superheated metal is solidified as it flows downstream which is the effect of the mold and the post mold cooling. The copper mold is usually water-cooled whereas the post-mold cooling is done with water spraying. Solidified shell is continuously withdrawn from the exit of the mold. Hence we have a thermal transport from a continuously moving material. When the metal shell is formed, it shrinks due to phase change as well as subcooling. Metal shrinkage leads to an air gap at the metal-mold interface. This hampers the heat extraction efficiency of the mold.

Figure 2 shows the complete geometry of the mold with dimensional parameters. As stated earlier, aluminum was chosen for the cast material while copper was selected as the mold material. The pre-mold region was assumed to be insulated whereas the mold surface and the post mold region was subjected to convective heat transfer. Aluminum was modeled as Newtonian incompressible fluid with Boussinesque approximation. The fluid flow was assumed to be laminar and two-dimensional. The symmetry of the problem allowed for modeling half of the domain for computational purposes. The left half of the domain was modeled and a transient algorithm was used. The mold wall exit was taken as the origin. Hence the metal flows in the negative Y direction.

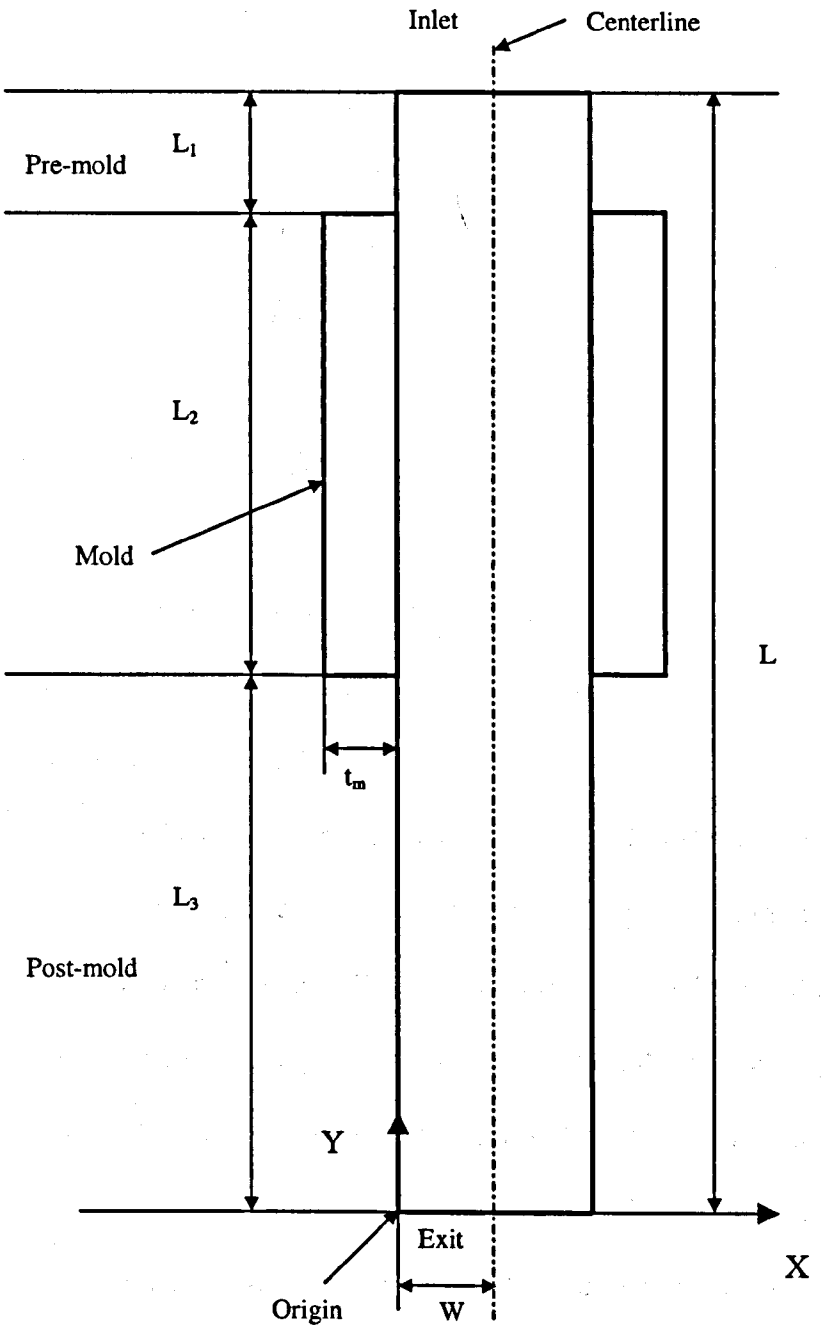

Figure 2. Problem domain in terms of dimensional parameters.

The aspect ratio is defined as:

$$Ar = L / W = 20 \tag{2.1}$$

Various mold parameters shown in Figure 2 are defined as follows:

$$L_3 / L = 0.5 \tag{2.2}$$

$$L_1 / L = 0.1 \tag{2.3}$$

$$t_m / W = 0.25 \tag{2.4}$$

where,

L_1 = length of the pre-mold region.

L_2 = length of the mold.

L_3 = length of the post mold or the secondary mold.

W = half width of the cast material.

t_m = thickness of the copper mold.

A commercial finite element code called Ansys (1999) was used for the numerical investigation. Although the code solves for a single-phase fluid, a user routine was developed to include multiphase fluid flow accompanied by solidification. The user routine was validated with analytical and experimental information to gain confidence in the method. The ultimate objective was to study the effect of air gap formation on the interfacial heat transfer. Consequently, the original algorithm was then modified to include interfacial heat resistance to model the air gap formation. The algorithm is explained in detail in the following chapter. Numerical simulations were conducted on a Silicon Graphics Inc. (SGI) Origin 200 server.

Enthalpy based formulation

During recent years, much interest has been devoted to the numerical analysis of problems involving nonlinear phase change, a phenomenon which takes place in many processes of technological interest to include solidification of various forming processes, freezing problems, applications to solar energy and applications to castings. While for certain materials phase change occurs over a wide band of temperature range thus allowing realistic computational approximations to physically model the situations; for several other materials the phase change phenomenon takes place with almost no temperature variation (a Dirac-δ-type behavior), thereby making such problems more difficult to deal with computationally. Present code (*Ansys*) employs the enthalpy method to tackle the phase change problem which is briefly outlined in this section.

A physical quantity, namely enthalpy, is introduced which is defined as the integral of the heat capacity with respect to temperature and is sufficiently smooth even over the phase change interval. Tamma and Raju (1990) pointed out that the temperature based formulations were ineffective in handling abrupt variations in heat capacity and these formulations approach to approximate heat capacity in the phase change zone. They also observed that the enthalpy methods were more natural in eliminating some of these hindrances to an extent, but still experience some of the same difficulties. The root of the problem was either in accurately representing the temperature distribution, locating the phase front, or both.

Enthalpy is defined as the integral of heat capacity with respect to temperature. Thus,

$$H = \int_{T_0}^{T} \rho \cdot C(T) dT \tag{2.5}$$

or equivalently,

$$\frac{dH}{dT} = \rho \cdot C(T) \tag{2.6}$$

The derivative in the above equation is numerically averaged over each element, from which the value of ρC is obtained.

The enthalpy method incorporates the latent heat in the specific heat of the material. Referring to Figure 3, the typical heat capacity is given by:

$$\rho \cdot C(T) = C_s \qquad \text{for } T_0 < T < T_1 \tag{2.7}$$

$$\rho \cdot C(T) = \rho \cdot C^* = \rho \cdot (\frac{L_h}{\Delta T}) \qquad \text{for } T_1 < T < T_2 \tag{2.8}$$

$$\rho \cdot C(T) = \rho \cdot C_l \qquad \text{for } T_2 < T \tag{2.9}$$

where T_0 = Reference temperature.

ΔT = Phase change interval. Phase transition zone is the temperature difference over which the evolution of latent heat takes place in the enthalpy method.

T_1 = Solidus temperature.

T_2 = Liquidus temperature.

The latent heat of the material is embedded in the adjusted specific heat C^* over the temperature range ΔT.

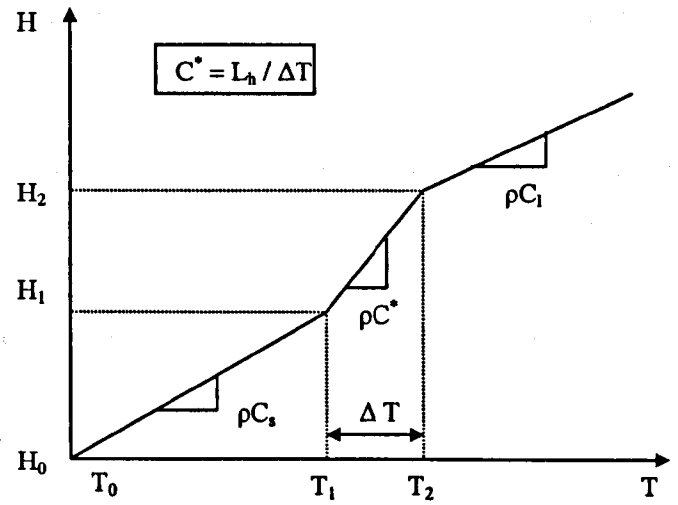

Figure 3. Typical enthalpy versus temperature plot in phase change problem.

For pure metals, solidification is assumed to occur over a finite temperature interval despite isothermal phase change. This phase change range must be kept small to avoid large deviation from the original solidification problem. Additionally, it is quite possible that the temperature at a node may skip the phase change interval in a single iteration if the time step is too large or the grid is not dense enough. Hence, the problem entails careful control of mesh and time stepping.

Rather than direct evaluation of the heat capacity, the enthalpy is interpolated according to:

$$H = N_i(x_i) \cdot H_i(t) \tag{2.10}$$

In equation (2.10), H_i and N_i are the enthalpy values at the nodes and the usual interpolation functions within an element respectively. The heat flow formulation involving solidification employed by the present code is briefly outlined in the following section.

Applying the law of conservation of energy over a differential control area without heat generation we get,

$$\rho \cdot C \cdot (\frac{\partial T}{\partial t} + \{v\}^T \cdot \{L\} \cdot T) = \{L\}^T \cdot ([D] \cdot \{L\} \cdot T) \tag{2.11}$$

where: ρ = Density

C = Specific heat

T = Temperature

t = Time

$$\{L\} = \text{vector operator} = \begin{Bmatrix} \frac{\partial}{\partial x} \\ \frac{\partial}{\partial y} \end{Bmatrix}$$

$$\{v\} = \text{velocity vector for mass transport of heat} = \begin{Bmatrix} v_x \\ v_y \end{Bmatrix}$$

$$[D] = \text{conductivity matrix} = \begin{bmatrix} k_x & 0 \\ 0 & 0 \end{bmatrix}$$

The common form of equation (2.11) can be written as

$$\frac{\partial(\rho C_p T)}{\partial t}+\frac{\partial(\rho V_x C_p T)}{\partial x}+\frac{\partial(\rho V_y C_p T)}{\partial y}=\frac{\partial}{\partial x}\left(k\frac{\partial T}{\partial x}\right)+\frac{\partial}{\partial y}\left(k\frac{\partial T}{\partial y}\right) \qquad (2.12)$$

Specified convection over surface S can be represented as:

$$\{q\}^T\{\eta\}=-h(T_\infty-T_s) \qquad (2.13)$$

where: $\{q\}$ = heat flux

$\{\eta\}$ = unit outward normal vector

T_∞ = ambient temperature.

T_s = temperature at the surface S of the model

h = coefficient of convective heat transfer.

It should be noted that positive heat flow is into the boundary.

Equation (2.11) is pre-multiplied by a virtual change in temperature δT and integrated over the area of the element to give:

$$\int_{Area}\left(\rho\cdot C\cdot\delta T\left(\frac{\partial T}{\partial t}+\{v\}^T\{L\}T\right)+\{L\}^T(\partial T)[D]\{L\}T\right)d(area)=\int_S \delta T\cdot T\cdot h(T_\infty-T)d(S) \qquad (2.14)$$

where: Area = area of the element

δT = an allowable virtual temperature (= $\delta T(x,y,t)$)

and S = surface of the model where convection is applied.

Since T varies over space and time, it can be written as:

$$T = \{N\}^T \{T_e\} \tag{2.15}$$

where: T = T(x,y,t) = temperature

{N} = {N(x,y)} = element shape functions

$\{T_e\} = \{T_e(t)\}$ = nodal temperature vector

The time derivative of equation (2.15) can be written as:

$$\dot{T} = \frac{\partial T}{\partial t} = \{N\}^T \left\{\dot{T}_e\right\} \tag{2.16}$$

δT also has the form:

$$\delta T = \{\delta T_e\}^T \{N\} \tag{2.17}$$

Further, using equation (2.15), we have:

$$\{L\}T = [B]\{T_e\} \tag{2.18}$$

where: $[B] = \{L\}\{N\}^T$

Substituting equations (2.13), (2.15), (2.16), (2.17) and (2.18) in equation (2.14), we get:

$$\int_{Area} \rho \cdot C\{N\}\{N\}^T d(Area)\left\{\dot{T}_e\right\} + \int_{Area} \rho \cdot C\{N\}\{v\}^T [B] d(Area)\{T_e\} +$$

$$+ \int_{Area} [B]^T [D][B] d(Area)\{T_e\} = \int_S T_\infty \cdot h \cdot \{N\} d(S) - \int_S h \cdot \{N\} \cdot \{N\}^T \{T_e\} \cdot d(S)$$

(2.19)

Gathering the coefficient of the terms $\left\{\dot{T}_e\right\}$ and $\{T_e\}$ on the left hand side, the equation (2.19) can be represented as:

$$[C_e^t]\left\{\dot{T}_e\right\} + \left([K_e^m] + [K_e^b] + [K_e^c]\right)\{T_e\} = \{Q_e^c\} \tag{2.20}$$

where: $[C_e^t] = \int_{Area} \rho \cdot C\{N\}\{N\}^T d(Area)$ = Element specific heat matrix.

$[K_e^m] = \int_{Area} \rho \cdot C\{N\}\{v\}^T [B] d(Area)$ = Element mass transport conductivity matrix.

$[K_e^b] = \int_{Area} [B]^T [D][B] d(Area)$ = Element diffusion conductivity matrix

$[K_e^c] = \int_S h \cdot \{N\} \cdot \{N\}^T \cdot d(S)$ = Element convection surface conductivity matrix.

$[Q_e^c] = \int_S T_\infty \cdot h \cdot \{N\} d(S)$ = Element convection heat flow vector.

Thus equation (2.20) represents the final form which is solved in each iteration. In this equation the element specific heat matrix $[C_e^t]$ is evaluated from the enthalpy curve for the solidification problem. Hence, referring to Figure 3, the enthalpy values needed to be input with respect to some reference value to get the enthalpy variation to deal with the phase change. A detailed version of the enthalpy formulation could be found in Ansys (1999) and the publication of Namburu and Tamma (1990).

Governing Equations

In this section, the laws governing the problem are elucidated in terms of mathematical expressions. The governing equations are subjected to the boundary conditions of the problem to formulate a solution. These expressions would then be discretized using the finite element approach to estimate the solution. The present problem involved thermal transport with conductive and convective heat transfer. The mold and the post mold were subjected to convective heat transfer whereas conduction was present throughout the domain. As discussed earlier, the solidification was handled by introducing latent heat evolution in the specific heat of the material using the enthalpy method.

Assumptions about the fluid and the analysis are as follows:

1. The fluid is Newtonian, incompressible with Boussinesque approximation.
2. The fluid flow is laminar in the liquid region.
3. There is negligible change in the density with change in phase.
4. Materials were considered homogeneous and isotropic.
5. Material properties were constant within individual phases.
6. Viscous work and viscous dissipation is neglected.
7. In the phase transition zone (ΔT), the thermal conductivity of the domain is equal to the thermal conductivity of the solid phase. In the enthalpy method, evolution of latent heat takes place in the phase transition zone.

The problem is defined by the laws of conservation of mass, momentum and energy which are stated in the following section. These laws are expressed in terms of partial differential equations which are discretized with a finite element technique.

Continuity Equation

From the conservation of mass law comes the continuity equation:

$$\frac{\partial(V_x)}{\partial x}+\frac{\partial(V_y)}{\partial y}=0 \tag{2.21}$$

where:

V_x and V_y = components of the velocity vector in the x and y direction, respectively.

x, y = global Cartesian coordinates.

t = time.

Momentum Equations

The momentum equations, commonly known as the Navier-Stokes equations, govern the fluid flow and are given by:

$$\rho\frac{\partial V_x}{\partial t}+\rho V_x\frac{\partial V_x}{\partial x}+\rho V_y\frac{\partial V_x}{\partial y}=-\frac{\partial P}{\partial x}+\mu\left[\frac{\partial^2 V_x}{\partial x^2}+\frac{\partial^2 V_x}{\partial y^2}\right] \tag{2.22}$$

$$\rho\frac{\partial V_y}{\partial t}+\rho V_x\frac{\partial V_y}{\partial x}+\rho V_y\frac{\partial V_y}{\partial y}=-\frac{\partial P}{\partial y}+\mu\left[\frac{\partial^2 V_y}{\partial x^2}+\frac{\partial^2 V_y}{\partial y^2}\right]+\rho g_y\beta(T-T_\infty) \tag{2.23}$$

Equations (2.22) and (2.23) represent the momentum equation in x and y directions respectively.

Energy equation

The energy equation governs the heat transfer and is given by:

$$\rho C\left[\frac{\partial T}{\partial t}+V_x\frac{\partial T}{\partial x}+V_y\frac{\partial T}{\partial y}\right]=k\left[\frac{\partial^2 T}{\partial x^2}+\frac{\partial^2 T}{\partial y^2}\right] \tag{2.24}$$

The energy equation is the thermal transport equation. As stated earlier, the density of the liquid is constant throughout the domain but subject to the Boussinesque approximation and the specific heat and the thermal conductivity are evaluated according to their respective phases in the domain.

The momentum equation is coupled with the energy equation. In the liquid region the velocity terms are assembled with the appropriate values from the velocity vector field obtained from the solution of momentum equations to get the temperature field. In the solid phase, the X component of velocity is set to zero whereas the withdrawal speed $-U_0$ is substituted for the Y velocity component to account for thermal transport. Thus, the only governing equation in the solid phase is the energy equation. The equations (2.21) through (2.24) are subjected to boundary conditions, which are described in the following section.

Boundary conditions.

The governing equations along with the boundary conditions define the problem completely. The boundary conditions are dictated by various assumptions stated in the previous section of governing equations. Referring to Figure 2, it should be noted that only the left half of the domain was modeled due to symmetry of the problem. The origin is set at the exit of mold wall.

The boundary conditions in dimensional parameters are as follows:

Mold inlet:

At $y = 0; 0 \leq x \leq W$:

$V_x = 0, V_y = -U_0, T = T_0$.

Centerline (axis of symmetry):

At $x = W; 0 \leq y \leq L$:

$V_x = 0, \partial T / \partial x = 0$.

Pre-mold region:

At $x = 0; 0 \leq y \leq L_1$:

$V_x = 0, V_y = 0, \partial T / \partial x = 0$.

Post-mold region:

At $x = 0; (L_1 + L_2) \leq y \leq L$:

$V_x = 0, V_y = 0, H_3$ (convective heat transfer coefficient).

Mold exit:

At $y = L; 0 \leq x \leq W$:

$V_x = 0, V_y = -U_0, \partial T / \partial y = 0$.

Copper mold surface:

At $y = L_1$ and $-t_m \leq x \leq 0$; $y = (L_1 + L_2)$ and $-t_m \leq x \leq 0$; $x = -t_m$ and $L_1 \leq y \leq (L_1 + L_2)$:

H_2 (convective heat transfer coefficient).

The pre-mold is insulated whereas the copper mold and the post-mold region are subjected to surface convection. The metal enters the mold inlet at the superheat temperature and there is no axial heat transfer at the mold exit. Also, there is no heat and mass transfer across mold centerline which is the axis of symmetry. The mold walls are subjected to the no slip boundary condition and the mold entry as well as the exit is subjected to constant withdrawal velocity boundary condition.

Initial conditions:

Initially, the metal is supposed to be at superheat temperature and flowing at withdrawal speed throughout the domain.

At time $t = 0$;

For the entire domain: $T = T_0$, $V_x = 0$ and $V_y = -U_0$.

Non-dimensionalization of Governing Equations

The governing equations were non-dimensionalized by defining basic non-dimensional parameters which are outlined in this section. The following equations define the non-dimensional parameters:

$$X^* = \frac{x}{W} \tag{2.25}$$

$$Y^* = \frac{y}{W} \tag{2.26}$$

$$V_x^* = \frac{V_x}{W}, \; V_y^* = \frac{V_y}{W} \tag{2.27}$$

$$P^* = \frac{P}{U_0^2 \cdot \rho} \tag{2.28}$$

$$\theta = \frac{T - T_\infty}{T_s - T_\infty} \tag{2.29}$$

$$t^* = \frac{U_0 \cdot t}{W} \tag{2.30}$$

where: x, y = linear dimensions

V_x, V_y = velocity components in the x and y directions respectively

U_0 = withdrawal velocity

W = half thickness of the cast material

P = pressure

T_∞, T_s = ambient temperature and solidification temperature respectively

In equations (2.25) through (2.30), the superscript (*) is used to define the corresponding non-dimensional parameter. Standard non-dimensional numbers used for the non-dimensionalization of governing equations are stated as follows:

$$\mathrm{Re} = \frac{\rho \cdot U_0 \cdot W}{\mu} \tag{2.31}$$

$$\mathrm{Pr} = \frac{\mu \cdot C}{k} \tag{2.32}$$

$$Gr = \frac{g_y \beta \cdot \rho^2 \cdot W^3 (T - T_\infty)}{\mu^2} \tag{2.33}$$

$$Pe = \mathrm{Re} \cdot \mathrm{Pr} \tag{2.34}$$

$$Ste = \frac{C_s (T_s - T_\infty)}{L_h} \tag{2.35}$$

Substituting equations (2.25) through (2.35) in the governing equations (2.21) through (2.24), we get,

$$\frac{\partial V_x^*}{\partial X^*} + \frac{\partial V_y^*}{\partial Y^*} = 0 \tag{2.36}$$

$$\frac{\partial V_x^*}{\partial t^*} + V_x^* \frac{\partial V_x^*}{\partial X^*} + V_y^* \frac{\partial V_x^*}{\partial Y^*} = -\frac{\partial P^*}{\partial X^*} + \frac{1}{\mathrm{Re}} \left[\frac{\partial^2 V_x^*}{\partial X^{*2}} + \frac{\partial^2 V_x^*}{\partial Y^{*2}} \right] \tag{2.37}$$

$$\frac{\partial V_y^*}{\partial t^*} + V_x^* \frac{\partial V_y^*}{\partial X^*} + V_y^* \frac{\partial V_y^*}{\partial Y^*} = -\frac{\partial P^*}{\partial Y^*} + \frac{1}{\mathrm{Re}} \left[\frac{\partial^2 V_y^*}{\partial X^{*2}} + \frac{\partial^2 V_y^*}{\partial Y^{*2}} \right] + \frac{Gr}{\mathrm{Re}^2} \theta \tag{2.38}$$

$$\frac{\partial \theta}{\partial t^*} + V_x^* \frac{\partial \theta}{\partial X^*} + V_y^* \frac{\partial \theta}{\partial Y^*} = \frac{1}{Pe} \left[\frac{\partial^2 \theta}{\partial X^{*2}} + \frac{\partial^2 \theta}{\partial Y^{*2}} \right] \tag{2.39}$$

Equations (2.36) through (2.39) are the governing equations in the non-dimensional form for the present problem. The governing equations along with the non-dimensional boundary conditions which are defined in the following section, represent a complete set which define the problem of continuous casting.

Non-dimensional Boundary Conditions

The boundary conditions were non-dimensionalized in a similar manner to the govenring equations by using the same non-dimensional parameters as defined in the earlier section.

The boundary conditions in the non-dimensional form are as follows:

Mold inlet:

At $Y^* = L/W$; $0 \leq X^* \leq 1$:

- $V_x^* = 0$, $V_y^* = -1$, $\theta = \theta_0$.

Centerline (axis of symmetry):

At $X^* = 1$; $0 \leq Y^* \leq L/W$:

- $V_x^* = 0$, $\partial\theta / \partial X^* = 0$.

Pre-mold region:

At $X^* = 0$; $(L_2 + L_3)/W \leq Y^* \leq L/W$:

- $V_x^* = 0$, $V_y^* = 0$, $Bi_1 = 0$

Post-mold region:

At $X^* = 0$; $0 \leq Y^* \leq L_3/W$:

- $V_x^* = 0$, $V_y^* = 0$, Bi_3 (convection)

Mold exit:

At $Y^* = 0$; $0 \leq X^* \leq 1$:

- $V_x^* = 0$, $V_y^* = -1$, $\partial\theta / \partial Y^* = 0$.

Copper mold surface:

At $Y^* = L_3/W$ and $-t_m/W \leq X^* \leq 0$; $Y^* = (L_2 + L_3)/W$ and $-t_m/W \leq X^* \leq 0$; $X^* = -t_m/W$ and $L_3/W \leq Y^* \leq (L_2 + L_3)/W$:

- Bi_2 (convection)

To summarize, the mold wall was subjected to a no-slip velocity boundary condition ($V_x^* = 0$, $V_y^* = 0$), whereas the entry and the exit of the mold have a constant withdrawal velocity boundary condition ($V_y^* = -1$). The X- component of the velocity is zero at the centerline ($V_x^* = 0$). Boundary condition of the second kind was applied to the pre-mold, centerline ($\partial\theta / \partial X^* = 0$) and the mold exit ($\partial\theta / \partial Y^* = 0$) as regards the temperature. The metal enters the mold at superheated temperature ($\theta = \theta_0$) and the mold and the post mold surfaces are subjected to convective heat transfer defined by Biot number, Bi_2 and Bi_3, respectively.

Table 2. Thermophysical properties of aluminum and copper.

Property	Liquid aluminum	Solid aluminum	Copper
Density, kg/m^3	2542.5	2542.5	8933
Specific Heat, J/kg K	1080	1076	385
Viscosity, kg/m s	1.3×10^{-3}	-	-
Thermal Conductivity, W/m K	94.03	238	401
Thermal Expansion, /K	1.2×10^{-4}	-	-
Latent heat of fusion, J/kg	3.95×10^{5}	-	-
Phase change temperature, K	933.5	933.52	-

CHAPTER 3

NUMERICAL METHOD

Over the past five decades, solutions to the problem of phase change have been attempted with the help of analytical, semi-empirical and numerical techniques. Numerical techniques can be categorized into finite difference, finite element and finite volume approaches. Finite element analysis seems to have an edge over the other approaches due to its relative ease in handling abrupt non-linearities in material properties. The enthalpy method is one of the most powerful methods available to tackle a phase change problem. As pointed out by Tamma and Raju (1990), the enthalpy-based formulation offered a great potential and promise for numerical simulations of the phase change problem due to its inherent effectiveness in handling the evolution of latent heat.

In the present research, the enthalpy method has been adopted to model the continuous casting process, which was discussed in Chapter 2. This chapter briefly deals with the finite element formulation, user algorithm for continuous casting and the code validation. A computational matrix was set up to study the overall effect of each degree of freedom on the process. The basic algorithm was validated with published analytical and experimental information to benchmark the method. A commercial FEA software, Ansys (1999), was used for the numerical simulations. The following sections describe the element description as well as the finite element discretization.

Element Description

The element used for the present analysis was FLUID141 (Refer Ansys CFD Flotran analysis guide). Figure 4 shows FLUID141, which is a 4 node quad element (triangular 3 node element is also available as an option.). FLUID141 can be used to model transient or steady state fluid/thermal systems that involve fluid and/or non-fluid regions.

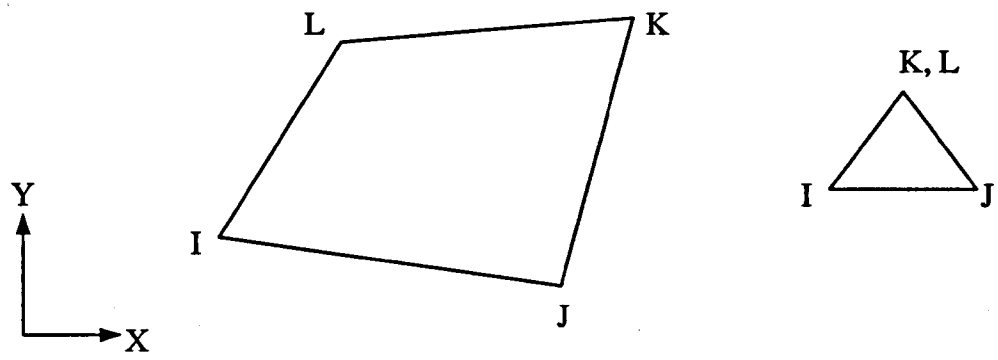

Figure 4. FLUID 141 Element, Ansys (1999)

The material properties defined using this element are density, viscosity, thermal conductivity and specific heat. In addition, enthalpy values at different temperatures need to be input in order to handle solidification. The properties can vary with respect to temperature. Velocities, temperature and pressure constitute the degrees of freedom. The momentum and the energy equation are coupled and are solved to get the velocity and the temperature fields.

It is often required to model systems involving the combination of fluid and non-fluid element, the present code models a maximum of 100 non-fluid elements. Only the

energy equation is solved in the non-fluid region. Material properties of the non-fluid elements include density, specific heat and thermal conductivity and their variation with temperature is permissible. Apart from these features, other user options include choosing turbulence models, different algebraic solvers, multiple species transport and rotating or stationary coordinate system. Detailed information on the models could be found in the Ansys (1999). Table 3 shows the input summary for the element.

Table 3. FLUID141 Input Summary

Element Name	FLUID141
Nodes	I, J, K, L
Degrees of Freedom	Velocities, Pressure, Temperature
Real Constants	See Real Constants. Refer Ansys (1999)
Material Properties	Non-fluid: Conductivity, Density, Specific Heat
	Fluid: Conductivity, Density, Specific heat, Viscosity
Surface Loads	Heat Flux, Convective heat transfer coeff, Radiation
Body Loads	Heat Generation, Force
Special Features	Nonlinear, Six turbulence models, Incompressible or compressible algorithm, transient or steady state algorithm, Rotating or stationary coordinate system, Algebraic solvers particular to FLOTRAN, Optional distributed resistance and fan models, Multiple species transport.
KEYOPT(1)	Activates multiple species transport. 0 - Species transport is not activated. 2 - 6 - Number of species transport equations to be solved
KEYOPT(3)	0 - Cartesian coordinates (default) 1 - Axisymmetric about Y-axis 2 - Axisymmetric about X-axis 3 - Polar Coordinates

Finite Element Formulation

The present code uses a sequential solution algorithm. This means that element matrices are formed, assembled and the resulting system solved for each degree of freedom separately. Development of the matrices proceeds in two parts. In the first, the form of the equations is achieved and an approach taken towards evaluating all the terms. Next, the algorithm is outlined and the element matrices are developed from the equations.

Discretization of the Equations:

The momentum and energy equation have the form of a scalar transport equation. There are four types of terms: transient, advection, diffusion and source. For the purpose of describing the discretization methods, variable ϕ is considered. The form of the scalar transport equation is:

$$\frac{\partial(\rho C_\phi \phi)}{\partial t}+\frac{\partial(\rho V_x C_\phi \phi)}{\partial x}+\frac{\partial(\rho V_y C_\phi \phi)}{\partial y}=\frac{\partial}{\partial x}\left(\Gamma_\phi \frac{\partial \phi}{\partial x}\right)+\frac{\partial}{\partial y}\left(\Gamma_\phi \frac{\partial \phi}{\partial y}\right)+S_\phi \qquad (3.1)$$

where

C_ϕ = transient and advection coefficient

Γ_ϕ = diffusion coefficient

S_ϕ = Source terms.

Table 4 shows the variables, coefficients and the source terms for the transport equations specific to this problem. Substituting the coefficients from Table 4. gives the governing

equations (2.21) through (2.24) for the present problem. The pressure equation is derived using the continuity equation. The development of the pressure equation can be found in the Ansys (1999). Since, the approach is the same for each equation, only the generic transport equation need be treated.

The discretization process, therefore, consists of deriving the element matrices to assemble the following matrix equation:

$$\left([A_e^{transient}]+[A_e^{advection}]+[A_e^{diffusion}]\right)\{\phi_e\}=\{S_e^{\phi}\} \tag{3.2}$$

Galerkin's method of weighted residuals is used to form the element integrals. The suffix e in above equation denotes the element.

Table 4. Transport equation representation specific to the current problem.

ϕ, Degree of freedom (DOF)	C_ϕ	Γ_ϕ	S_ϕ
V_x	1	μ	$-\partial P/\partial x$
V_y	1	μ	$-\partial P/\partial y+\rho\cdot g_y\cdot\beta(T-T\infty)$
T	C	k	0

Transient Term:

The first of the element matrix contributions is from the transient term and a lumped mass approximation is used. The general form is simply:

$$\left[A_e^{transient}\right] = \int W^e \frac{\partial(\rho \cdot C_\phi \phi)^e}{\partial t} d(vol) \tag{3.3}$$

A backward difference scheme is used to evaluate the transient derivative. On a nodal basis, the following implicit formulation is used. The current time step is the n^{th} time step and the expression involves the previous two time step results.

$$\frac{\partial(\phi)}{\partial t} = \frac{(\phi)_{n-2}}{2\Delta t} - \frac{4(\phi)_{n-1}}{2\Delta t} + \frac{3(\phi)_n}{2\Delta t} \tag{3.4}$$

The n^{th} time step produces a contribution to the diagonal of the element matrix, while the derivatives from the previous time step form contributions to the source term.

Advection Term:

The advection term is discretized using the monotone streamline upwind approach based on the idea that pure advection transport is along characteristic lines. In pure advection transport, one assumes that no transfer occurs across characteristic lines, i.e. all

transfer occurs along streamlines. Therefore, it can be assumed that the advection term as expressed in equation (3.5) is constant when expressed along a streamline.

$$\frac{\partial(\rho \cdot C_\phi V_x \phi)}{\partial x} + \frac{\partial(\rho \cdot C_\phi V_y \phi)}{\partial y} = \frac{\partial(\rho \cdot C_\phi V_s \phi)}{\partial S} \tag{3.5}$$

$$\left[A_e^{advection}\right] = \frac{d(\rho \cdot C_\phi V_s \phi)}{ds} \int W^e d(vol) \tag{3.6}$$

This formulation is made for every element, each of which will have only one node, which gets contributions from inside the element. The derivative is calculated using a simple difference (Refer to Figure 5.):

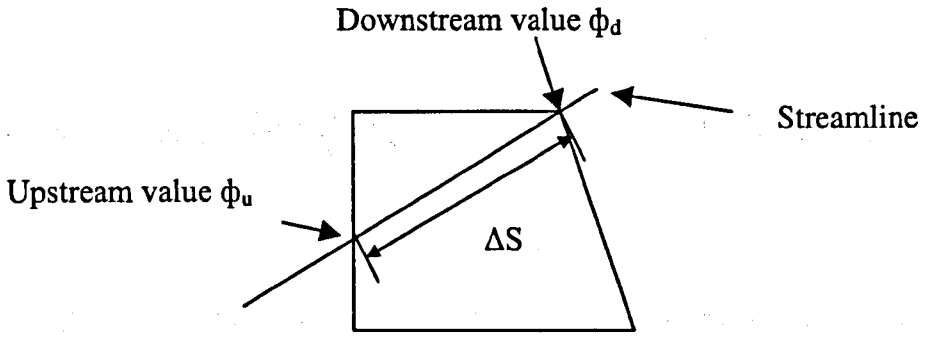

Figure 5. Streamline Upwind Approach over an element.

$$\frac{d(\rho \cdot C_\phi V_s \phi)}{ds} = \frac{(\rho \cdot C_\phi V_s \phi)_u - (\rho \cdot C_\phi V_s \phi)_d}{\Delta S} \tag{3.7}$$

The subscripts d and u represent the values at the downstream and the upstream nodes respectively. The process consists of cycling through all the elements and identifying the downwind nodes. A calculation is made based on the velocities to see where the streamline through the downwind node came from. Weighing factors are calculated based on the proximity of the upwind location to the neighboring nodes.

Diffusion Terms:

The expression for the diffusion terms comes from integration over the problem domain after the multiplication by the weighing function.

$$\text{Diffusion contribution} = \int W^e \frac{\partial}{\partial x}\left(\Gamma_\phi \frac{\partial \phi}{\partial x}\right) d(vol) + \int W^e \frac{\partial}{\partial y}\left(\Gamma_\phi \frac{\partial \phi}{\partial y}\right) d(vol) \tag{3.8}$$

The x and y terms are all treated in similar fashion. Therefore, the illustration is with the term in the x direction. An integration by parts is applied:

$$\int W^e \frac{\partial}{\partial x}\left(\Gamma_\phi \frac{\partial \phi}{\partial x}\right) d(vol) = \int \frac{\partial W^e}{\partial x} \Gamma_\phi \frac{\partial \phi}{\partial x} d(vol) \tag{3.9}$$

Once the derivative of ϕ is replaced by the nodal values and the derivatives of the weighting function, the nodal values will be removed from the integrals.

$$\frac{\partial \phi}{\partial x} = W_x^e \phi \tag{3.10}$$

$$W_x^e = \frac{\partial W^e}{\partial x} \tag{3.11}$$

The diffusion matrix may now be expressed as:

$$\left[A_e^{diffusion}\right] = \int W_x^e \Gamma_\phi W_x^e + W_y^e \Gamma_\phi W_y^e d(vol) \tag{3.12}$$

Source Terms:

The evaluation of the source terms consists of merely multiplying the source terms by the weighting function and integration over the volume.

$$S_\phi^e = \int W^e S_\phi d(vol) \tag{3.13}$$

The enthalpy method is used to model solidification which has been discussed in earlier chapter (Chapter 2).

Segregated Solution Algorithm:

Each degree of freedom is solved in sequential fashion. The equations are coupled, so that each equation is solved with intermediate values of the other degrees of freedom. The process of solving all the equations in turn and then updating the properties is called a global iteration.

The momentum equation is used to generate an expression for the velocity in terms of the pressure gradient. This is used in the continuity equation after it has been integrated by parts. The global iteration structure is shown in Figure 6. $V_x^{'}$ and $V_y^{'}$ are approximate velocities which are obtained by the initial solution of the momentum equations. These approximate values of the velocity components are used to formulate the pressure equation to obtain the pressure values in the liquid. The pressure solution along with the approximate values of the velocity components is used to get a refined velocity field. This velocity vector solution is finally used in the energy equation to get the temperature field. Finally, the global iteration terminates after updating the temperature dependent properties and a convergence check. The detailed exposition of the algorithm can be found in Ansys (1999).

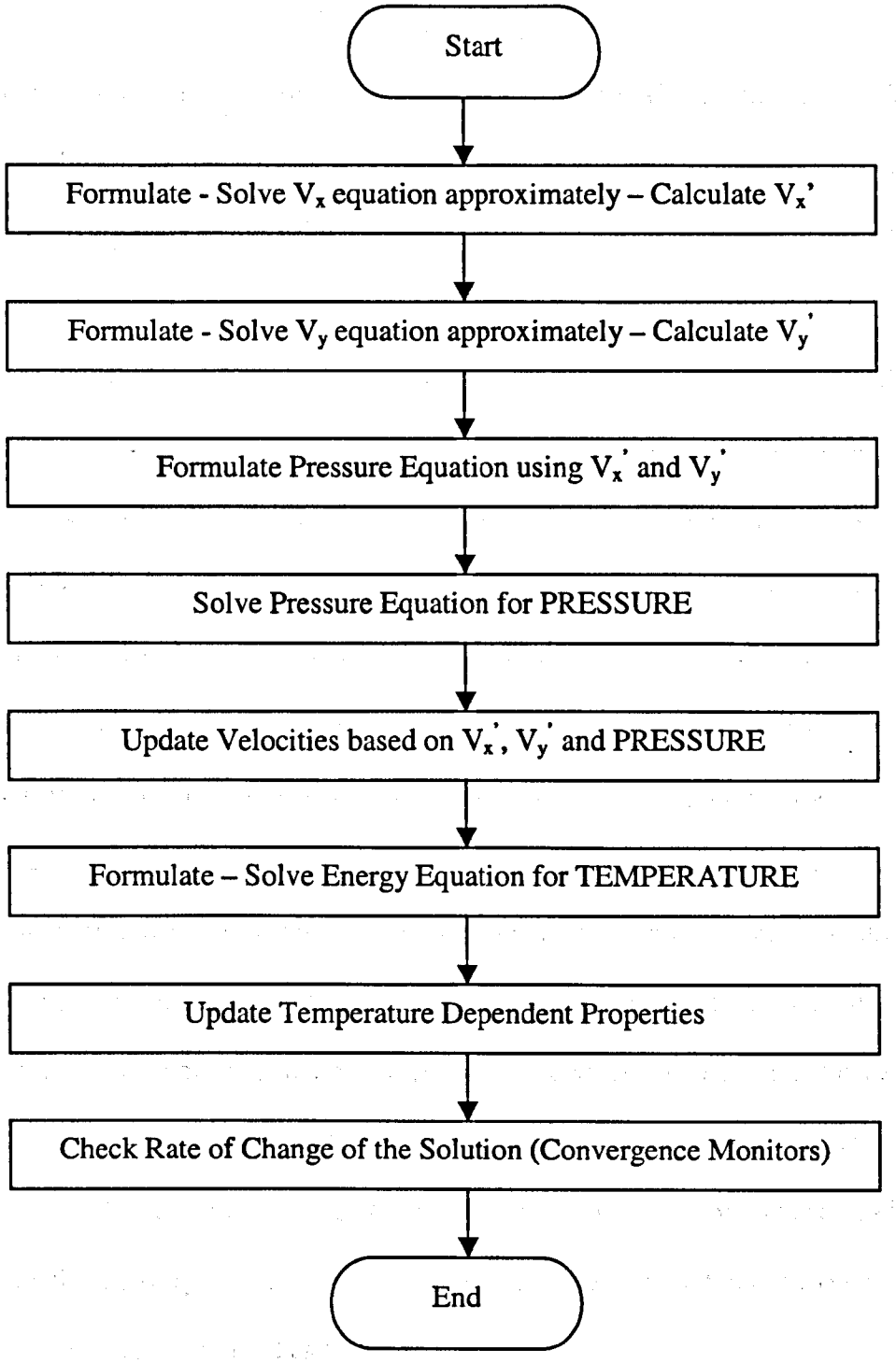

Figure 6. Global iteration structure of Ansys (1999).